Hindawi
Advances in Materials Science and Engineering
Volume 2022, Article ID 1235843, 17 pages
https://doi.org/10.1155/2022/1235843

Research Article

Bond Slip Behavior of Grout-Filled Concrete Members with Different Interface Materials

Eryu Zhu[1], **Teng Li**[1], **Lei Liu**[1], **Li Zhu**[1] **and Yuanyuan Tian**[1,2]

[1]*Civil and Environmental Building, Deptartment of Civil Engineering, Beijing Jiaotong University, Shangyuancun 3rd, Beijing 100044, China*
[2]*China Railway Fifth Survey and Design Institute Group Co., Ltd., Beijing 102600, China*

Correspondence should be addressed to Eryu Zhu; eyzhu@bjtu.edu.cn

Received 18 November 2021; Accepted 21 March 2022; Published 11 April 2022

Academic Editor: Junjie Wang

The present paper investigates the relationship between pressure (bond stress) and displacement at the failure load for different materials through testing and modeling. First, single-end tests were conducted on prebonded stressed and perforated concrete specimens with corrugated plastic, metal, and rubber extractive pipes. These tests reveal that corrugated plastic pipes provide good bonding performance with concrete and grout. Hence, they can be applied in the hole-forming process of posttensioned prestressed bonded structures, along with corrugated metal pipes and rubber extractive pipes. Based on the experimental observations and results, a theoretical approach for applying corrugated plastic pipes in projects such as China's high-speed rail has finally been demonstrated.

1. Introduction

In recent years, field investigations of posttensioned prestressed bonded concrete box girders in China have revealed some quality issues, such as the durability of prestressed bonded systems, which is identified as a significant problem. Applying prestressed bonding first requires forming holes using pipe materials for the most widely used post-tensioned prestressed bonded concrete structures. Therefore, hole-forming materials have become indispensable for post-tensioned prestressed bonded systems. Three main types of hole-forming materials used in posttensioning are nowadays used: corrugated metal pipes, corrugated plastic pipes, and rubber extractive pipes. Among these types, rubber extractive pipes are the most commonly used materials, followed by corrugated metal pipes and corrugated plastic pipes.

However, the engineering community is still concerned about applying corrugated plastic pipes [1]. Plastic corrugated pipes have a slightly lower bonding performance with concrete and grout than metal corrugated pipes, and they are prone to delamination, which causes overall structural body peeling along the delamination surfaces or cracking problems due to concrete spalling. This seriously affects the durability of the prebonded stress structure and is crucial for the use of corrugated plastic pipes for pre-bonded stress concrete railway bridges.

In 1986, the Swiss company VSL [2] first proposed a hole-forming material, corrugated plastic pipes, for post-tensioned, prestressed holes and vacuum-assisted compression processes. Corrugated plastic pipes are a new type of hole-forming material based on corrugated metal pipes. They possess high-density polyethylene (HDPE), the base material [3]. Compared to corrugated metal pipes, these pipes have good corrosion resistance and antiaging properties. The friction coefficient of the pipe is about 0.14, which is a lot smaller than that of the corrugated metal pipes. The pipe's strength is enough to keep the material from getting damaged while pouring concrete. Furthermore, they are also good in permeability and sealing performance, which makes them suitable for vacuum grouting. Their high fatigue resistance leads to good performance and longer service life for the whole structure. However, as reported in existing literature [4], corrugated plastic pipes have poor ductility and

are readily bent due to their low elastic modulus and strength [5]; thus, corrugated plastic pipes are not used in high-speed railway projects.

An adequate bond between prestressed tendons and concrete can be achieved by effective bonding between prestressed tendons and grout, grout and corrugated pipes, and corrugated pipes and concrete [1]. The bonding between corrugated pipes and concrete has a significant impact on the safety performance of high-speed rail. Most of the existing studies included tests on the bond-slip of steel reinforcement, fiber-reinforced polymers (FRPs), and others such as concrete and steel [5], cement grout and steel [6, 7], FRP-reinforced concrete [6–9], different forms of steel pipes together with concrete [10, 11], and steel plates and concrete [12]. The existing experiments included pull-out tests [13] and double-lap shear tests [14]. The tests mainly considered the bond-slip properties between the bonded materials. In contrast, few of them reported the bonding properties of the inner and outer components using interface materials (such as corrugated plastic pipes, corrugated metal pipes, and rubber extractive pipes).

Corrugated plastic pipes were used as an intermediate interface material to test the bonding performance of a concrete member filled with grout. Multiple sets of single-end compression tests were designed in this study to investigate the performance of such specimens. In addition, pressure experiments were conducted on specimens with corrugated metal pipes and rubber extractive pipes as the hole-forming material to serve as comparative experiments. Considering the corrugated structure of the corrugated pipes and the large internal diameter, the overall performance of the grout-filled concrete specimens may be closer to that of concrete with steel pipes under pressure. Referring to the bond performance test of steel pipes [15], single-end compression tests were conducted on grout-filled concrete members with different interface materials. After 2–3 years of extensive experimental research supported by the China Railway Corporation, this paper reports a systematic study on the compression performance of internal grouts of structures of corrugated plastic pipes with concrete or grout structures. In addition, freeze-thaw cycle experiments with different cycles of −40 to 60°C were used to explore the effect of temperature. Finally, the effects of factors such as different contact lengths and contact areas on bond-slip performance were explored to investigate the suitability of corrugated plastic pipes in railway prestressed bonded concrete bridges. This study could significantly impact the development and application of the corrugated plastic pipe industry in China.

2. Experimental Program

2.1. Test Specimens. The experiments performed push-out tests on 27 specimens, including three corrugated metal pipe specimens, three rubber extractive pipe specimens, and 21 corrugated plastic pipe specimens with different parameters in seven groups. The details of the four groups of specimens are presented in Table 1. The length of one corrugated unit of the corrugated material was 45 mm. D represents the inner diameter of the hole, L represents the bond length, H represents the crest height of the corrugated pipes, and T represents the thickness of the corrugated material.

The cross-sectional dimensions of the corrugated plastic pipe specimen are shown in Figure 1, where D is the inner diameter of the pipe, and L is the bond length between the interface material and concrete or grout. The dimensions of all specimens are detailed in Table 1, in which the label "P-90-135-1" defines a grout-filled concrete member with a corrugated plastic pipe as the interface material, with an inner diameter of 90 mm and a bond length of 135 mm. "1" represents the No. 1 specimen in each group. In other cases, "M" means specimens with a corrugated metal pipe as the interface material. "R" means specimens with rubber extractive pipe as the interface material. "FTC-10-1" means the No. 1 specimen in the group of 10 times of the freeze-thaw cycle.

Each test specimen was a cylinder with an outer diameter of 400 mm. A steel mold with an inner diameter of 400 mm and a height of 180 mm was selected, and a rectangular iron block was welded to the center of the mold bottom to locate the pipe. The bond lengths between the corrugated pipes and concrete were determined for each specimen before fabricating them. Specimen preparation is shown in Figure 2. The bond length between the corrugated pipes and concrete was adjusted with foam blocks of different lengths at the free end. The concrete was selected as the C50. The gap between the mold and the corrugated pipe was coated with glass glue. A nylon bag was inserted into the corrugated pipes to prevent leakage and concrete from entering the inside of the corrugated pipes, which would impact the test findings. The corrugated plastic pipes were fixed in the mold as required, and lubricating oil was applied inside the steel mold for easy demolding. The concrete was mechanically mixed for a few minutes, poured into the test mold, and vibrated with a vibrator bar to ensure that the concrete was dense at the bottom of the embedded part and the load-bearing plate of the prestressed bonded tendon and the exposed surface was smooth. When pouring concrete, a 150 mm × 150 mm × 150 mm cubic standard test block was reserved for each concrete batch to determine its mechanical properties. After the concrete was wholly vibrated, the grout was mixed, and the specimens were uniformly grouted. The test specimens and standard test blocks were maintained in a special maintenance room to ensure the development of the early strength of the concrete and prevent dry shrinkage cracks. Water was poured once in the morning and once in the afternoon for the first 14 days. Tests were performed after 28 days.

2.2. Material Properties. The material properties of the concrete were determined using compressive concrete cube tests. Concrete cubes with a nominal side length of 150 mm were produced using standard mixing and curing techniques [16, 17]. The elastic modulus of concrete was measured according to the specification "Test Methods of Cement and Concrete for Highway Engineering" [18]. The material properties of concrete are listed in Table 2.

Table 1: Geometric parameters of grout-filled concrete members.

Specimen	Temperature (°C)	Freeze-thaw cycles	D (mm)	L (mm)	H (mm)	T (mm)	$D/45$	$L/45$
P-90-135-1			90	135	5.0	2.5	2.0	3.0
P-90-135-2			90	135	5.0	2.5	2.0	3.0
P-90-135-3			90	135	5.0	2.5	2.0	3.0
M-90-135-1			90	135	2.5	0.3	2.0	3.0
M-90-135-2			90	135	2.5	0.3	2.0	3.0
M-90-135-3			90	135	2.5	0.3	2.0	3.0
R-90-135-1			90	135			2.0	3.0
R-90-135-2			90	135			2.0	3.0
R-90-135-3			90	135			2.0	3.0
P-90-135-FTC-10-1	−40~60	10	90	135	5.0	2.5	2.0	3.0
P-90-135-FTC-10-2	−40~60	10	90	135	5.0	2.5	2.0	3.0
P-90-135-FTC-10-3	−40~60	10	90	135	5.0	2.5	2.0	3.0
P-90-135-FTC-20-1	−40~60	20	90	135	5.0	2.5	2.0	3.0
P-90-135-FTC-20-2	−40~60	20	90	135	5.0	2.5	2.0	3.0
P-90-135-FTC-20-3	−40~60	20	90	135	5.0	2.5	2.0	3.0
P-90-90-1			90	90	5.0	2.5	2.0	2.0
P-90-90-2			90	90	5.0	2.5	2.0	2.0
P-90-90-3			90	90	5.0	2.5	2.0	2.0
P-90-180-1			90	180	5.0	2.5	2.0	4.0
P-90-180-2			90	180	5.0	2.5	2.0	4.0
P-90-180-3			90	180	5.0	2.5	2.0	4.0
P-80-120-1			80	120	5.0	2.5	1.8	2.7
P-80-120-2			80	120	5.0	2.5	1.8	2.7
P-80-120-3			80	120	5.0	2.5	1.8	2.7
P-110-165-1			110	165	5.0	2.5	2.4	3.7
P-110-165-2			110	165	5.0	2.5	2.4	3.7
P-110-165-3			110	165	5.0	2.5	2.4	3.7

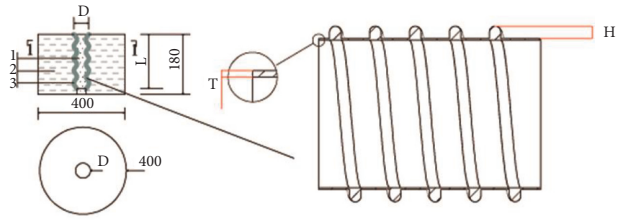

Figure 1: Specimen size and pipe size (mm). 1-Grout, 2-Concrete, 3-Pipe material.

(a) (b) (c) (d)

Figure 2: Specimen preparation, (a) Pour concrete, (b) Clean inside space, (c) Un-grouted specimen, (d) Grouted specimen.

The grout met the requirements of TB/T3192 [19], and its proportion was cement: water: admixture = 1 : 0.35 : 0.09, where the cement was ordinary silicate cement with a strength grade of 52.5 MPa. The grout met the following conditions: initial setting time higher than 4 h, final setting time less than 24 h, 30 min flow rate less than or equal to 30, and 24 h free bleeding rate of 0. According to GB/T 17671 1999 [20], the compressive strength test was conducted for

Table 2: Concrete properties.

	1	2	3	4	5	6	7	Mean	Standard deviation
Concrete cube strength (MPa)	61.5	62.2	63.1	59.2	58.8	60.5	59.4	60.7	1.5
Elasticity modulus (10^4 MPa)	3.9	4.1	3.6	4.1	3.7	3.9	3.7	3.9	0.2

40 mm × 40 mm × 160 mm specimens using a compressive strength testing machine. The grout's 28-day strength tests yielded 56.5, 59.3, and 61.4 MPa, with a mean of 59.07 MPa and a standard deviation of 2.007 MPa, meeting the requirements for strength greater than or equal to 50 MPa.

The specifications of the corrugated plastic pipes given by the factory are φ90 with an elastic modulus of 800 MPa, tensile yield bond stress of 17 MPa, a density of 900 kg/m^3, and Poisson's ratio of 0.35. The specification of corrugated metal pipes is φ90 with an elastic modulus of 2.06×10^5 MPa, tensile yield bond stress of 260 MPa, a density of 7850 kg/m^3, and Poisson's ratio of 0.30. The specifications of the rubber extractive pipes are φ90 with a fixed tensile strength of 6 MPa, the tensile strength of 12 MPa, elongation at break of 350%, and shore A hardness of 65.

The tensile yield bond stress and elongation at break of corrugated plastic pipes were determined according to the specification GB/T 8804.1 2003 [21], and the results are shown in Table 3.

2.3. Test Setup. In this study, all tests were conducted under a computer-controlled compression machine with a capacity of 2000 kN. Geometric and physical alignments were conducted on the machine before applying the load. During the testing, the vertical load was applied only to the grout core, and subsequently, the grout core was pushed downward. A schematic of the test is shown in Figure 3. A compression machine directly provided the displacement at the loading end of the grout. The displacement at the bottom of the grout was measured using a displacement meter, which was the free end and was fixed on the lower steel bearing. Considering that the steel bearing may cause deviations in the test results, the steel support was loaded. When the loading force was 200 kN, the deformation of the steel support was approximately 0.01 mm, which was much smaller than the test value, so the influence of the steel bearing was ignored. The test pieces were pre-loaded before the official tests with a loading of 20 kN. For safety reasons, the force was loaded step-by-step. The loading process is computer-controlled, at a speed of 100 N/s. Each 100 kN load would last for one minute. The load was continuously applied until the specimen cracked or damaged or the displacement meter reading suddenly increased.

2.4. Freeze-Thaw Cycle. Bridges with prestressed corrugated plastic pipes with bonds for hole-forming are influenced by the annual spring, summer, fall, and winter temperature cycles. As the linear expansion coefficients of corrugated plastic pipes, concrete, and grout are very different, when the temperature changes, there may be large relative deformation and temperature bond stress between corrugated plastic pipes and concrete, affecting the bonding force between them. This test evaluated the impact of high and low temperature cycles on corrugated plastic pipes and concrete bonding performance by setting different temperature cycles. The range of temperature cycles set in this test ranged from −40°C to 60°C. To fully consider the range of temperature variation transferred from the bridge to the corrugated plastic pipes, a 2 h temperature holding operation was performed in the temperature box as the temperature increased or decreased. The temperature box is shown in Figure 4. The temperature inside the specimen was consistent with that outside the specimen during the experiment. As the temperature box was subjected to a limited external load, the specimens were first removed from the temperature box when the loading test was performed. Nine concrete test blocks in three groups were designed for this test. The numbers of cycles were 0, 10, and 20.

Table 3: Corrugated plastic pipe properties.

Specimen	Tensile strength (MPa)	Elongation at break (%)
1	15.8	251.5
2	17.6	287.5
3	17.9	268.1
Mean	17.1	269.0
Standard deviation	0.9	14.7

3. Results and Discussions

3.1. Axial Load-Displacement and Axial Load-Average Bond Stress Curves. Four sets of comparative tests were designed to analyze the bonding performance between corrugated plastic pipes and concrete or grout based on different test objectives. The experimental results are presented in Table 4. The ending criteria of the test were specimen failure or sudden increase in the displacement meter readings during the loading test. At this time, the displacement produced by the free end of the grout was different. At this point, most of the specimens were in the initial rise stage and reached the peak plateau stage.

The experimental results for each group are plotted in Figure 5, where for (a), the horizontal axis represents the inner grout-loaded end displacement (S), and the vertical axis represents the axial load (P). For (b), the horizontal axis represents the inner grout-loaded end displacement (S), and the vertical axis represents the average bond stress τ, defined in equation (1). P_u is the peak loading force of the specimen at the highest platform; τ_u is the peak average bond stress of the specimen at the highest platform; S_u is the displacement at the loading end just at the end of the first rising section of the bond stress curve of the specimen.

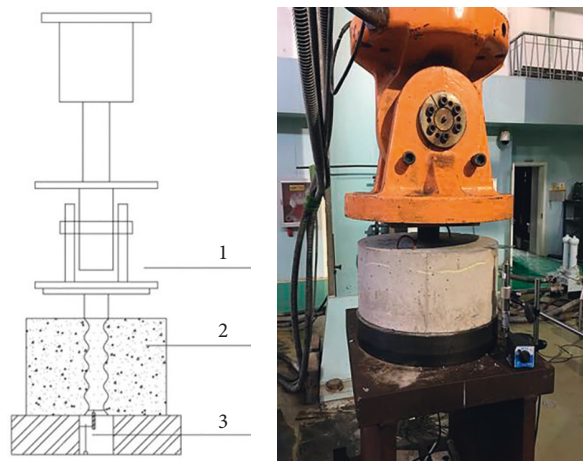

(a) (b)

Figure 3: Test setup, (a) schematic diagram, (b) Real test setup. 1-Compression machine, 2-Specimen, 3-Displacement meter.

Figure 4: Temperature box.

The average bond stress is calculated by [22]

$$\tau = \frac{P}{\pi d l}. \quad (1)$$

The initial slope is defined as the slope of the elastic stage curve between the origin (0, 0) and the turning point [23]. The slope consists of two types, one for the $P - S$ curve and the other for the $\tau - S$ curve.

Table 4: All specimens' compression load, bond stress, and critical displacements.

Group	Test ID	P_u (kN)	τ_u (MPa)	$\overline{P}$ (kN)	$\overline{\tau}$ (MPa)	k_τ
1	P-90-135-1	129.0	3.4	200.7	5.3	4.0
	P-90-135-2	251.9	6.6			
	P-90-135-3	221.0	5.8			
2	M-90-135-1	301.6	7.9	317.5	8.3	10.5
	M-90-135-2	400.0	10.5			
	M-90-135-3	250.8	6.6			
3	R-90-135-1	138.9	3.6	133.6	3.6	9.3
	R-90-135-2	130.2	3.4			
	R-90-135-3	131.7	3.5			
4	P-90-135-FTC-10-1	142.0	3.7	184.1	4.8	5.2
	P-90-135-FTC-10-2	231.7	6.1			
	P-90-135-FTC-10-3	178.6	4.7			
5	P-90-135-FTC-20-1	133.6	3.5	175.6	4.6	6.3
	P-90-135-FTC-20-2	204.2	5.3			
	P-90-135-FTC-20-3	188.9	4.9			
6	P-90-90-1	111.9	4.4	134.5	5.3	5.5
	P-90-90-2	139.9	5.5			
	P-90-90-3	151.7	5.9			
7	P-90-180-1	221.4	4.4	214.3	4.2	4.0
	P-90-180-2	207.1	4.1			
8	P-80-120-1	99.5	3.3	151.4	5.0	5.9
	P-80-120-2	202.9	6.7			
	P-80-120-3	151.7	5.0			
9	P-110-165-1	294.2	5.2	294.2	5.2	5.6
	P-110-165-2	351.8	6.2			
	P-110-165-3	236.6	4.2			

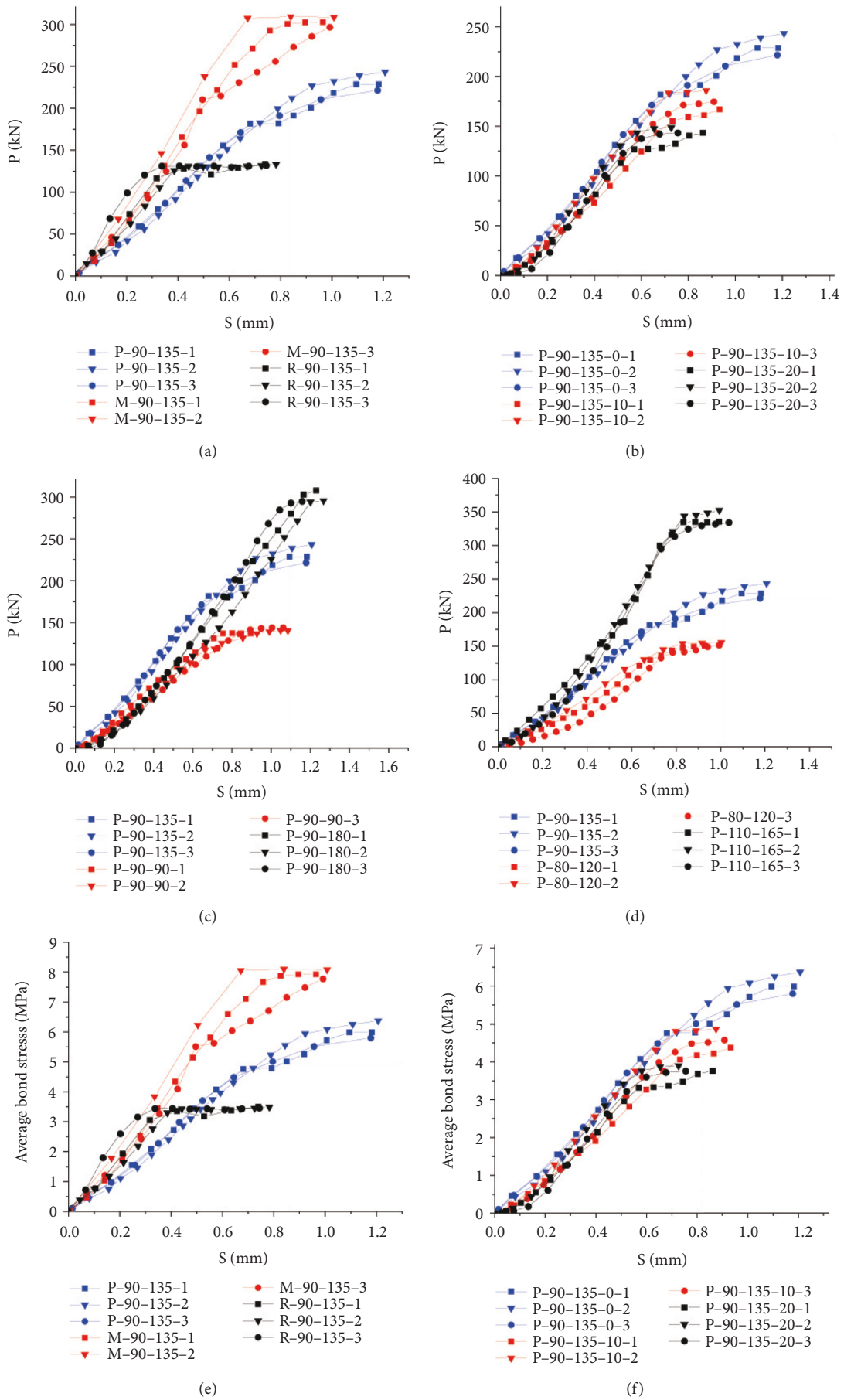

Figure 5: Continued.

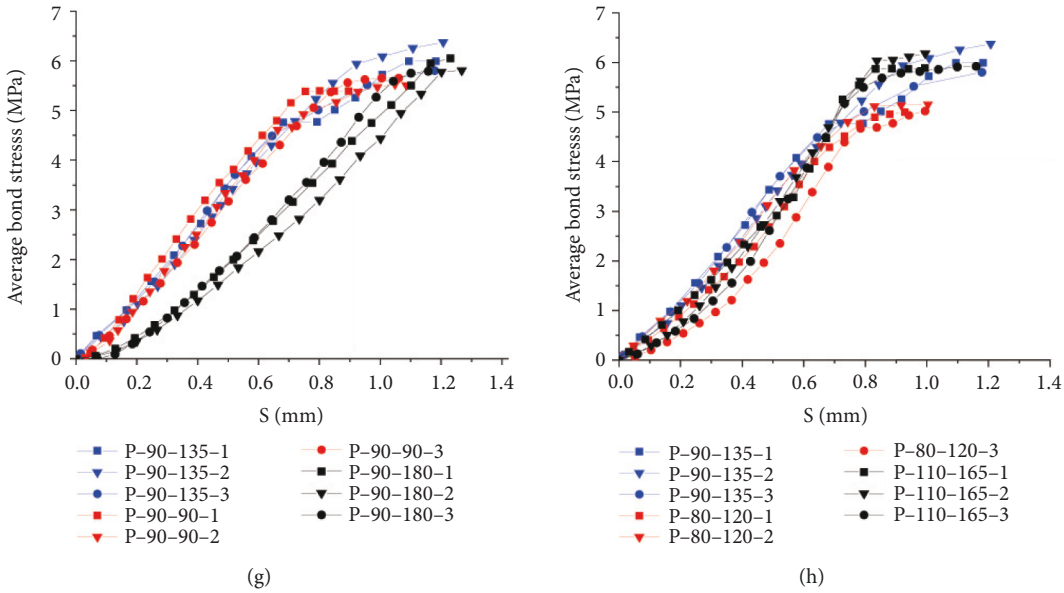

Figure 5: Bond-slip test results.

$$k_\tau = \frac{\overline{\tau_{u1}}}{\overline{s_{u1}}},$$
$$k_p = \frac{\overline{P_{u1}}}{\overline{s_{u1}}}. \quad (2)$$

The following conclusions can be drawn from existing studies [24]: the higher the bond stress is, the better the overall working performance is. The smaller the slip at the loading end is, the better bonding performance is. The higher the bond stiffness is, the higher the ratio of bond strength to bond-slip before the concrete is internally cracked is, and the higher the ability of different materials is to work together. In this study, the ranking of bonding performance of different hole-forming material specimens was evaluated by comparing different groups of specimens on various metrics in the conclusion section.

Results with error bars are shown in Figure 6.

In the experimental results, the curves for all specimens reached the peak plateau because the loading was interrupted when the specimens failed. Typical curves are of two types, as shown in Figure 7. The first type of two-segment curve shown in Figure 7(a) is the most common, in which the first segment of the curve is roughly an exponential distribution, and the second segment is a straight line. As for AB1 in Figure 7(a), the axial load of the specimen remains constant after reaching the peak. This is because the contact surface is rougher at this type of curve, resulting in more interlock and adhesive forces than the initial interface friction. Therefore, only the friction remained as the bonding force when the axial load peaked, and the dynamic friction remained almost constant. As for AB2 in Figure 7(a), the axial load of the specimen increases almost linearly after the first segment. This is because the interlock forces still remain in these specimens. Thus with the increase of slip, the axial load gradually increases.

In contrast, the second type of curve shown in Figure 7(b) is fewer in number. The axial load or stress of the second type of specimen reached its peak with a negative exponential distribution. It then increased linearly for a period, after which it increased as a quadratic function to a new peak and then remained constant. This specimen's interlocking force and adhesive force are smaller than the initial interface friction [10]. Therefore, when the axial load peaks for the first time, the friction force peaks and the interlocking force or adhesive force are still present at the interface, resulting in a gradual increase in the axial load. The load or stress peaks again when the interlocking or adhesive force disappears.

3.2. Influence of Materials on Bond-Slip. Corrugated plastic, rubber extractive, and corrugated metal pipes are the three main hole-forming materials for posttensioned prestressed bridges with bonds [25]. They have the same inner diameter. Although the parameters of the three materials themselves are different, the working conditions of the three forming methods are the same. Therefore, it is possible to compare them under the same conditions.

The bond-slip curves for the three sets of specimens corresponding to the three different hole-forming materials are shown in Figure 5, where (a) is the loading force-loaded end displacement curve and (b) is the average bond stress of the bond-loaded end displacement curve.

Of these, the specimens using rubber extractive pipes for hole-forming only had the first type of curve. The specimens using corrugated metal pipes for hole-forming had both types of curves. The specimens using corrugated plastic pipes for hole-forming had both types of curves.

As shown in Figure 5(b), the bond-slip for all three materials can be roughly divided into two phases: the first phase is roughly a linear rise, and the second phase is a peak

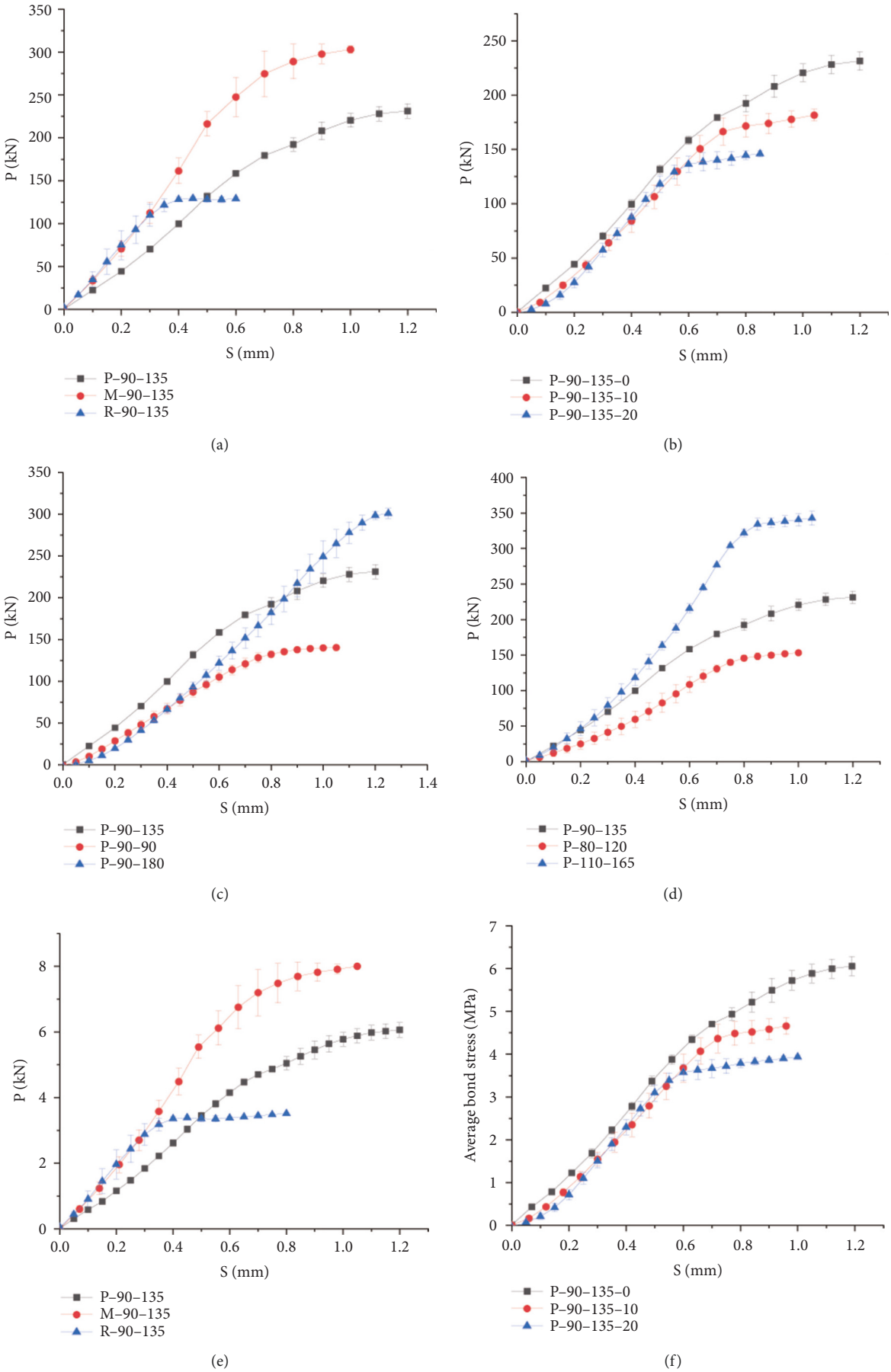

Figure 6: Continued.

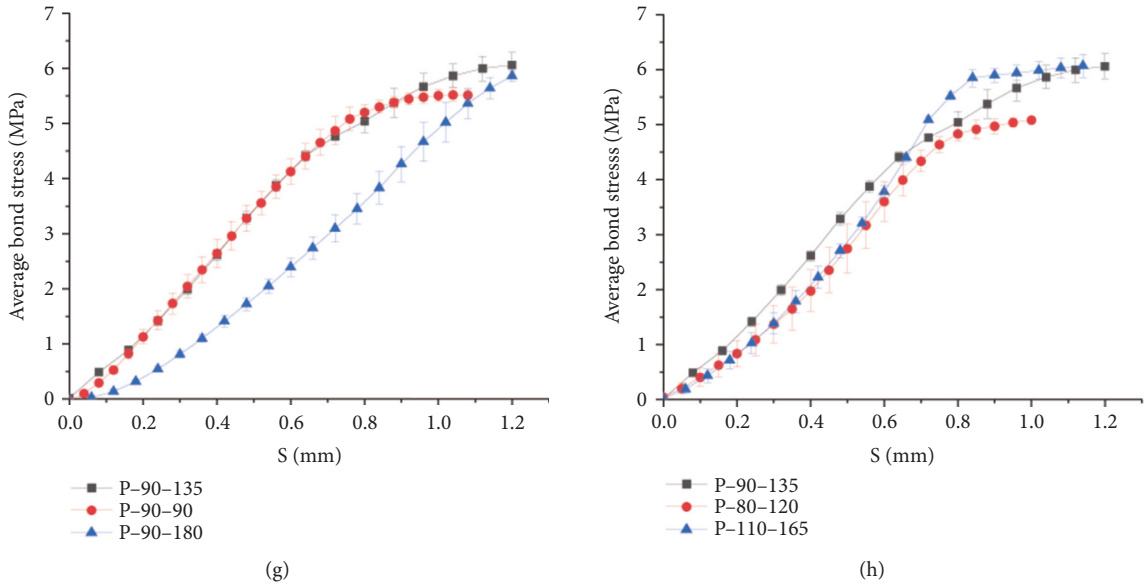

Figure 6: Bond-slip test results with error bars.

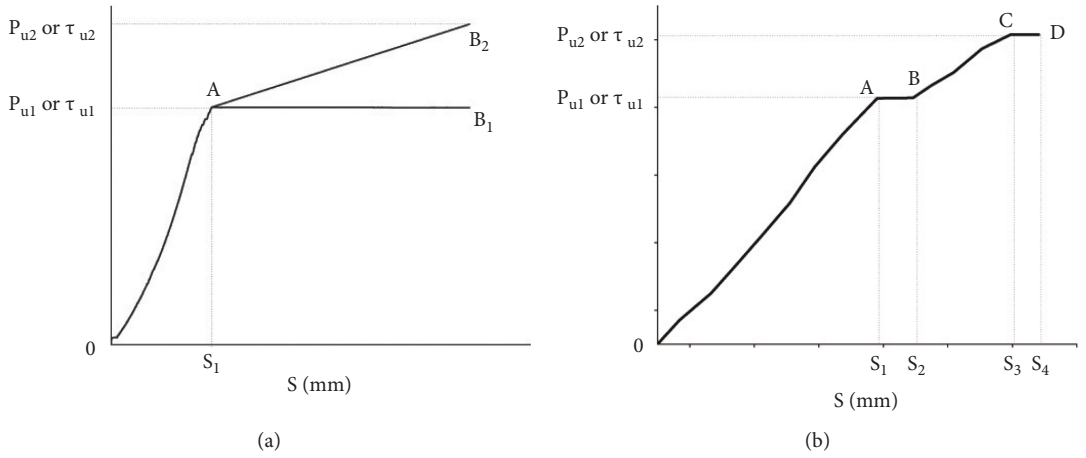

Figure 7: Curve types. (a) Type I curve, (b) Type II curve.

plateau phase or a linearly rising phase. Stiffness is considered the ability of different specimens to resist slip. Thus, the higher the stiffness, the higher is the force required to produce the same amount of slip. Comparing the slope of the pressure curve and that of the bond stress curve, the corrugated metal pipe specimen and the rubber extractive pipe specimen curves have similar slopes (stiffness). However, they are significantly higher than the corrugated plastic pipe specimen. This indicates that the corrugated metal pipes and the rubber extractive pipe specimens produced a stronger resistance to slip in the first stage. In contrast, the corrugated plastic pipe specimens produced a weaker resistance to slip. The bonding force consists of the chemical bonding force, mechanical bite force, and friction [27]. The antislip forces are mainly chemical bonding and mechanical bite forces in the initial slip generation.

Wang. et al. [28] has achieved improved chemical bonding by the application of two groups of accelerators, Carbonates and bicarbonates in the concrete. Through analyzing the outcome, the implications of the two accelerators, sodium carbonate (Na_2CO_3) and sodium bicarbonate ($NaHCO_3$), on the properties of OPC paste demonstrate that both could improve the initial and final setting time of OPC paste, but the effect of the two accelerators on compressive strength was different. The rapid development of ettringite and the creation of $CaCO_3$ through interactions between the two with portlandite generated the enhanced strength at 1 and 7 days. Na^+ reduces the adhesion between C-S-H gels by replacing Ca_2^+, leading to a decrease in strength. $NaHCO_3$ was found to be a better accelerator than Na_2CO_3.

Wang et al. [29] have discovered that with the increase of $Ca(HCO_3)_2$ content, the final set time and extension degree

of cement decrease. Furthermore, the initial formation of ettringite and the transformation of ettringite could be achieved by adding $Ca(HCO_3)_2$. The $CaCO_3$, which is the product of the reaction of $Ca(HCO_3)_2$ and portlandite, has a better filling effect than the limestone powders. And too much $Ca(HCO_3)_2$ could cause harmful pores on concrete, which will reduce the performance of concrete.

The rubber extractive pipe has strong slip resistance. This is mainly because the concrete and the internal grout are in direct contact when the rubber extractive pipe is pulled out after the hole is formed. Thus, the contact surface between them is rougher, which produces a higher mechanical bite force. Compared to corrugated plastic pipes, mostly made of HDPE or polypropylene, the corrugated metal pipe specimens made of soft steel strip [26] have a higher chemical bonding force with the concrete and grout, explaining their superior slip resistance. In addition, from Figure 5, it can be seen that the slopes of almost all curves first increased and then decreased. The initial increase occurred because the mechanical bite between the materials increased as the loading force increased, and the friction also increased. Thus, the slope continued to increase. When the amount of slip reached a certain level, the chemical bonding force disappeared, the slip resistance decreased, and the slope of the curve decreased accordingly. When the curve reaches the turning point, the overall sliding between multiple materials is produced, and the chemical bonding force and mechanical bite force disappear entirely. The bonding force is mainly provided by the dynamic friction force, which remains constant during the relative sliding of the members.

Comparing the critical displacement S_u, in the initial linear phase, the rubber extractive pipe specimens have a critical displacement of approximately 0.33 mm, followed by corrugated metal pipe and corrugated plastic pipe specimens with critical displacements of around 0.64 mm and 0.75 mm. As a result, chemical bonding and mechanical bite force dissipate at a much smaller slip. However, the corrugated metal pipe between the grout and concrete is entirely in contact with both, creating a higher total chemical bonding and mechanical bite force. The corresponding displacement is high. However, the corrugated plastic pipe specimens produced the most significant displacement. One of its reasons is that the corrugated plastic pipe has a higher contact area with the concrete and grout. Furthermore, the corrugated plastic pipe is softer than the corrugated metal pipes, thus allowing more deformation during relative slip.

Comparing the peak platform bond stress τ_u, we found that the rubber extractive pipe specimens had the most negligible forces when reaching the peak platform, followed by corrugated plastic and corrugated metal pipes. The contact area between the corrugated pipes at the interface and the concrete and grout is greater than that of the rubber extractive pipe specimens with direct contact between the concrete and grout, resulting in a higher chemical bonding force. The corrugated metal pipe is a soft steel strip with a more rigid texture. Its chemical bonding and mechanical bite forces are more significant than the corrugated plastic pipe. The plastic bellows exhibit shear failure during the middle and late loading periods (Figure 8). The bonding

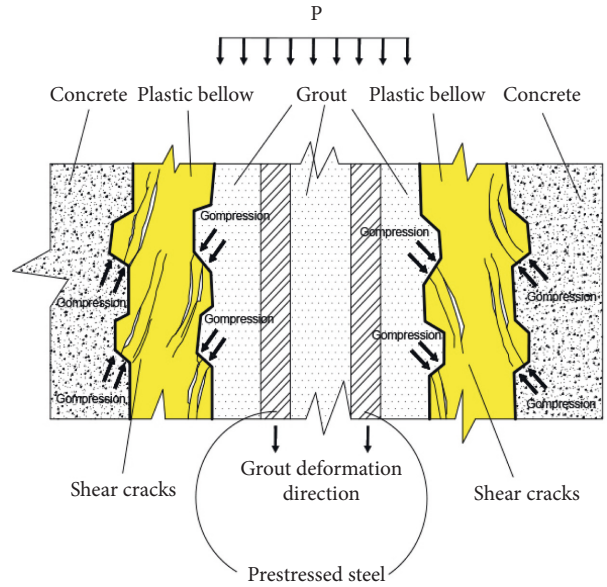

Figure 8: Inside pipe break.

stress of the plastic bellows specimen is higher than that of the rubber extractive pipe specimen because of the increased mechanical biting force between the broken bellows and concrete.

In summary, rubber extractive pipes have a comparable slope (slide resistance stiffness) to the corrugated metal pipe. Both are higher than those of the corrugated plastic pipes. Corrugated metal pipes have the highest peak bond stress, followed by corrugated plastic pipes and rubber extractive pipes; rubber extractive pipes have the smallest critical displacement, followed by corrugated metal pipes. The most significant value is for corrugated plastic pipes.

3.3. Influence of Freeze-Thaw Cycles on Bond-Slip. The corrugated plastic pipe concrete specimens did not show cracks after 10 and 20 freeze-thaw cycles in the temperature box without an external load. The corrugated plastic pipe did not detach or delaminate from the surrounding concrete or grout. This indicates that under a temperature cycle of −40°C to 60°C without load, the corrugated plastic pipes and concrete did not fail owing to the difference in deformation along the direction of the corrugated pipes owing to the difference in their linear expansion coefficients.

After checking the concrete specimens for cracks after freeze-thaw cycles, the corrugated plastic pipe concrete specimens were subjected to axial one-end compression. The test data were read, and the test results were processed.

From Figures 5, 9, 10 and Table 4, it can be seen that the average peak compressive loading force (bond stress) decreased by 8.54% after 10 freeze-thaw cycles and by 13.28% after 20 freeze-thaw cycles. In contrast, the average peak compressive loading force (bond stress) decreased by 5.19% after 20 freeze-thaw cycles compared to 10 freeze-thaw cycles. The data shows that the number of freeze-thaw cycles affects the bond performance, with a higher impact in the initial cycles and a decrease in impact strength in

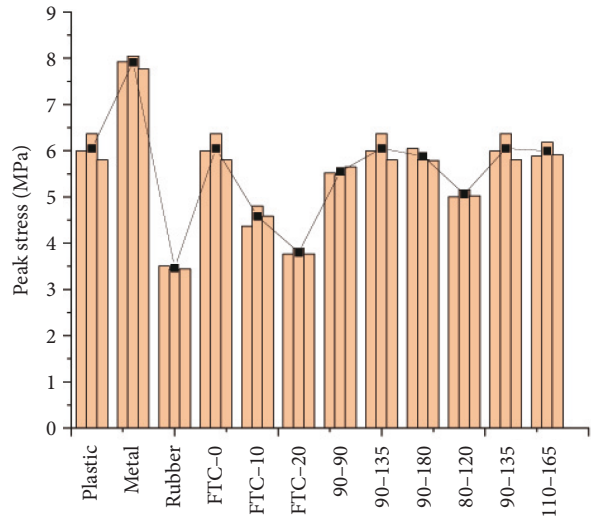

Figure 9: Peak stress comparison.

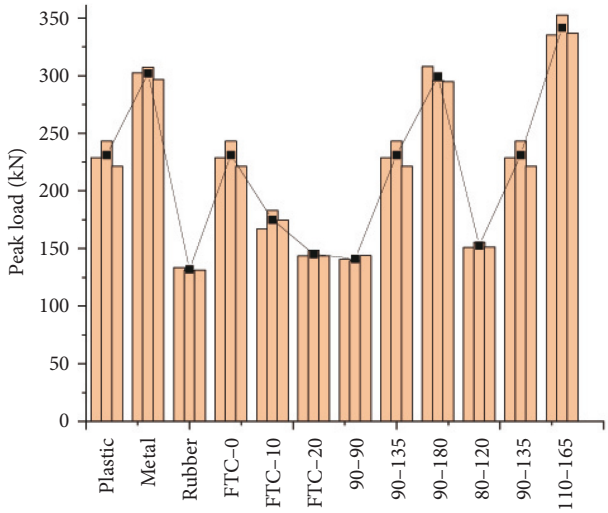

Figure 10: Peak load comparison.

later cycles. According to the existing literature [30], the length of the contact area is related to the transfer of stress across the interface. Eventually, the peak compressive loading force (bond stress) decreases as the number of freeze-thaw cycles increases. These increases cause a decrease in the effective stress transfer zone, which reduces the frictional force.

In contrast, according to the existing literature [27], freeze-thaw cycles cause deterioration of the concrete strength, which also leads to a decrease in the interfacial shear force. In other words, in actual projects, as the service life of prestressed bonded concrete railway bridges increases, the bond stress between corrugated plastic pipes and concrete or grout decreases, with significant changes in the first few years. However, the decreasing tendency decelerates as the service life increases. We also found that the initial stiffness continues to increase with an increase in the number of freeze-thaw cycles.

By observing the loading force and curve stiffness of bond stress (Figures 11 and 12), we found that the stiffness was the highest for 0 freeze-thaw cycles when the loading end displacement was less than approximately 0.3 mm, followed by 10 freeze-thaw cycles, and finally for specimens with 20 freeze-thaw cycles. Again, this was due to the reduction in chemical bonding forces caused by the freeze-thaw cycles. However, when the loading end displacement was higher than 0.3 mm, the slope increased the most with 20 freeze-thaw cycles, followed by specimens with 10 freeze-thaw cycles, and finally specimens with 0 freeze-thaw cycles.

Comparing the critical displacement S_u (Figure 13), we found that 10 freeze-thaw cycles had almost no effect on the results, with the displacement changing from 0.75 mm to 0.74 mm. However, the average critical displacement of the specimens after 20 freeze-thaw cycles was 0.59 mm. This indicates that the chemical bonding force decreases after 20 freeze-thaw cycles and that the displacement is smaller when the chemical bonding force disappears. This also shows a progressively significant effect after 20 freeze-thaw cycles.

3.4. Influence of Bond Length on Bond-Slip. In this study, the influence of the bond length on the bonding performance of corrugated plastic pipes with concrete or grout was considered. Under the same concrete strength, grout strength, inner diameter, and various parameters of corrugated plastic pipes, three types of specimens with bond lengths $l_a = d$, $l_a = 1.5d$ and $l_a = 2d$ were used, where d is the inner diameter of the corrugated plastic pipes ($d = 90$ mm). The bonding lengths were 90, 135, and 180 mm, respectively.

From Figure 5(a) and 10, it can be seen that as the bond length increases, the peak loading force of the specimen gradually increases. The increase in specimens with a bond length of 135 mm relative to specimens with a bond length of 90 mm was more significant than the increase in specimens with a bond length of 180 mm related to specimens with a bond length of 135 mm. The increase in loading force was due to the increase in bond length and the higher contact area between the internal and external materials; hence, there was a higher chemical bonding force, mechanical bite force, and friction between the materials. According to existing studies [31–34], when the bond length is less than a specific value, the peak loading force increases rapidly with increasing bond length; when the bond length is higher than a specific value, the increase in the peak loading force is no longer significant.

In addition, the intensity of the peak bond stress (Figure 9) of the specimen decreased with the increasing bond length. First, as the bond length increases, the contact area increases. According to formula (1), the bond stress is inversely proportional to the contact area; thus, the higher the bond length, the lower the bond stress of the peak bond. It can also be seen that the peak bond stresses for specimens with 90 mm and 135 mm bond lengths were close and significantly higher than the peak bond stress for specimens with a bond length of 180 mm. According to the conclusion above, the increase in peak loading force from the 135–180 mm bond length range was no longer significant. As

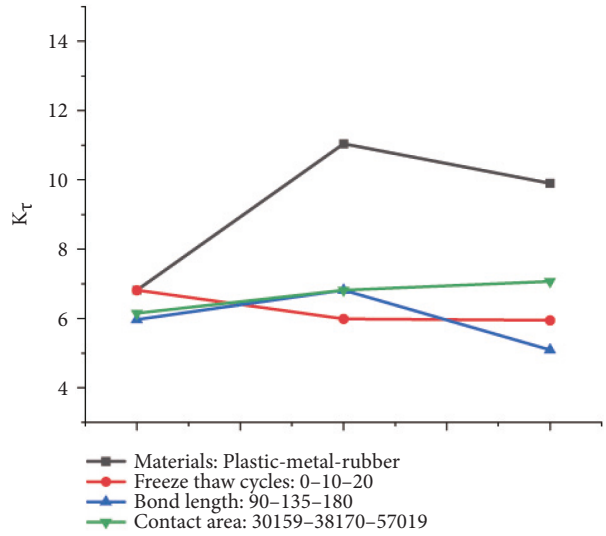

Figure 11: Stiffness (k_τ) comparison.

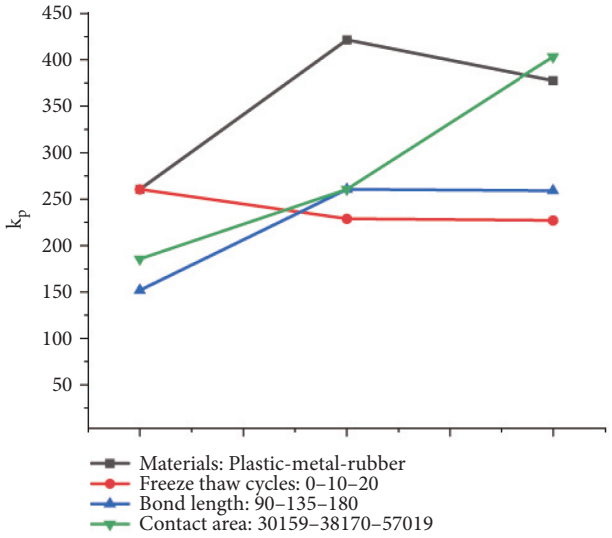

Figure 12: Stiffness (k_p) comparison.

the contact area considerably increased, the bond stress decreased considerably. Moreover, it can be seen that the initial stiffness decreased as the bond length increased.

Comparing the curve stiffness, we found that as the bond length increased, the force stiffness (Figure 12) first increased and then remained almost constant, whereas the stiffness of the bond stress curve (Figure 11) increased and then decreased. First, when the bond length changed from 90 to 135 mm, the contact area increased almost linearly for the force stiffness. The chemical bonding force and mechanical bite force also increase; thus, the stiffness increases. However, the stiffness remained unchanged when the bond length changed from 135 to 180 mm. This is possible because when the bond area increased linearly, the increase in chemical bonding force and mechanical bite force was comparable to the increase in force. However, observing the stiffness of the bond stress, we found that when the bond length changed from 90 to 135 mm, the contact area increased, and the chemical bonding force and mechanical bite force also increased considerably. Although the area also increased, the increase in the force was higher; thus, the stiffness increased. When the bond length changed from 135 to 180 mm, the area increased almost linearly and was inversely proportional to the bond stress. The increase in chemical bonding and mechanical bite forces was relatively small; thus, the stiffness decreased.

Comparing the critical displacement (Figure 13), we found that it gradually increased with increasing contact length, from 0.75 mm to 0.84 mm to 1.14 mm. This is mainly because a larger contact area produces a higher chemical bonding force and mechanical bite force. As a result, the chemical bonding and mechanical bite forces disappeared only after the internal grout displacement reached a sufficient level.

3.5. Influence of Contact Area on Bond-Slip. Formula (1) shows that under the same loading force P, bond stress τ, and inner diameter of the corrugated pipe d, the bond lengths of the corrugated pipe and concrete or grout l are inversely proportional. If the corrugated plastic pipe is assumed to be a hollow, smooth cylinder, then $\pi \cdot d \cdot l$ is the surface area of the hollow cylinder. In other words, the bond stress of the bond τ and the surface area of the hollow cylinder are inversely proportional. It can be seen that the contact areas between the corrugated plastic pipes and concrete or grout have a certain impact on the bond stress of bonds between corrugated plastic pipes and concrete or grout.

This test analyzes the effect of different contact areas of corrugated plastic pipes on the bond stresses, with all other conditions being the same. According to Figures 5, 10, and Table 4, the larger the bond area is, the greater the peak loading force is because of the larger contact area, and the greater the chemical bonding force, mechanical bite force, and friction force are. The friction force increases significantly. The peak bond stress (Figure 9) of specimens 80–120 was the smallest, followed by specimens 110–165 and 90–135. It is seen that the peak bond stress does not increase or decrease in one direction with increasing contact area. This may be because when the area is small, the various components of the bond force increase more as the area increases, increasing the bond stress. When the area exceeds a specific range, the increase in the components of the bond force is no longer significant, and the bond stress decreases.

In addition, the initial stiffness of both curves (Figures 11 and 12) increased as the bond area increased because each component of the bonding force increased. The critical displacement (Figure 13) also increased as the contact area increased. A larger contact area resulted in a higher chemical bonding force and a higher mechanical bite force. When these two forces disappear, the internal slip is relatively higher.

4. Theoretical Modeling

Only the initial rise phase of the bond stress-slip curve was studied because the post-ascent stage is complicated and cannot be predicted by a uniform function.

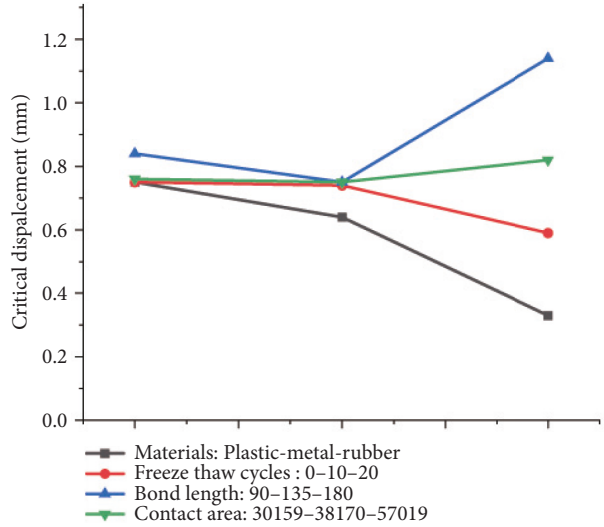

Figure 13: Critical displacement comparison.

Table 5: α values of different specimens.

Group	Test ID	τ_s	S_s	α
1	P-90-135-1	6.0	0.7	1.2
	P-90-135-2	6.4	0.9	1.1
	P-90-135-3	5.8	0.6	1.5
2	M-90-135-1	7.9	0.8	1.2
	M-90-135-2	8.1	0.7	1.2
	M-90-135-3	7.8	0.5	1.6
3	R-90-135-1	3.5	0.3	1.5
	R-90-135-2	3.4	0.4	1.3
	R-90-135-3	3.4	0.3	1.0
4	P-90-135-FTC-10-1	4.4	0.7	1.0
	P-90-135-FTC-10-2	4.8	0.7	1.1
	P-90-135-FTC-10-3	4.6	0.8	1.1
5	P-90-135-FTC-20-1	3.8	0.6	1.2
	P-90-135-FTC-20-2	3.9	0.6	1.0
	P-90-135-FTC-20-3	3.8	0.6	1.5
6	P-90-90-1	5.5	0.7	1.2
	P-90-90-2	5.5	0.9	1.0
	P-90-90-3	5.7	0.9	1.1
7	P-90-180-1	6.1	1.2	1.4
	P-90-180-2	5.8	1.2	1.5
	P-90-180-3	5.8	1.0	1.5
8	P-80-120-1	5.0	0.7	1.5
	P-80-120-2	5.2	0.8	1.0
	P-80-120-3	5.0	0.8	1.6
9	P-110-165-1	5.9	0.8	1.3
	P-110-165-2	6.2	0.8	1.4
	P-110-165-3	5.9	0.8	1.6

As the material properties of GFRP bars are similar to those of grout-filled pipes, the bond stress-slip relationship of GFRP bars in concrete was investigated to understand the bond behavior of the grout-filled concrete specimens. The BPE model proposed by Eligehausen et al. [35] is a classical model. This model was applied to the bond between steel bars and concrete and then successfully used to study the bond behavior between FRP bars and concrete by Rossetti et al. [36]. The bond stress-slip curve in this model is divided into different parts based on some representative parameters, such as the ultimate bond stress (τ_s), ultimate slip (S_s), and α.

Using curve-fitting on the experimental results of different specimens, the parameter α in this model was determined, as shown in Table 5.

Therefore, the bond stress-slip relationship in the curvilinear ascending branch is proposed as follows:

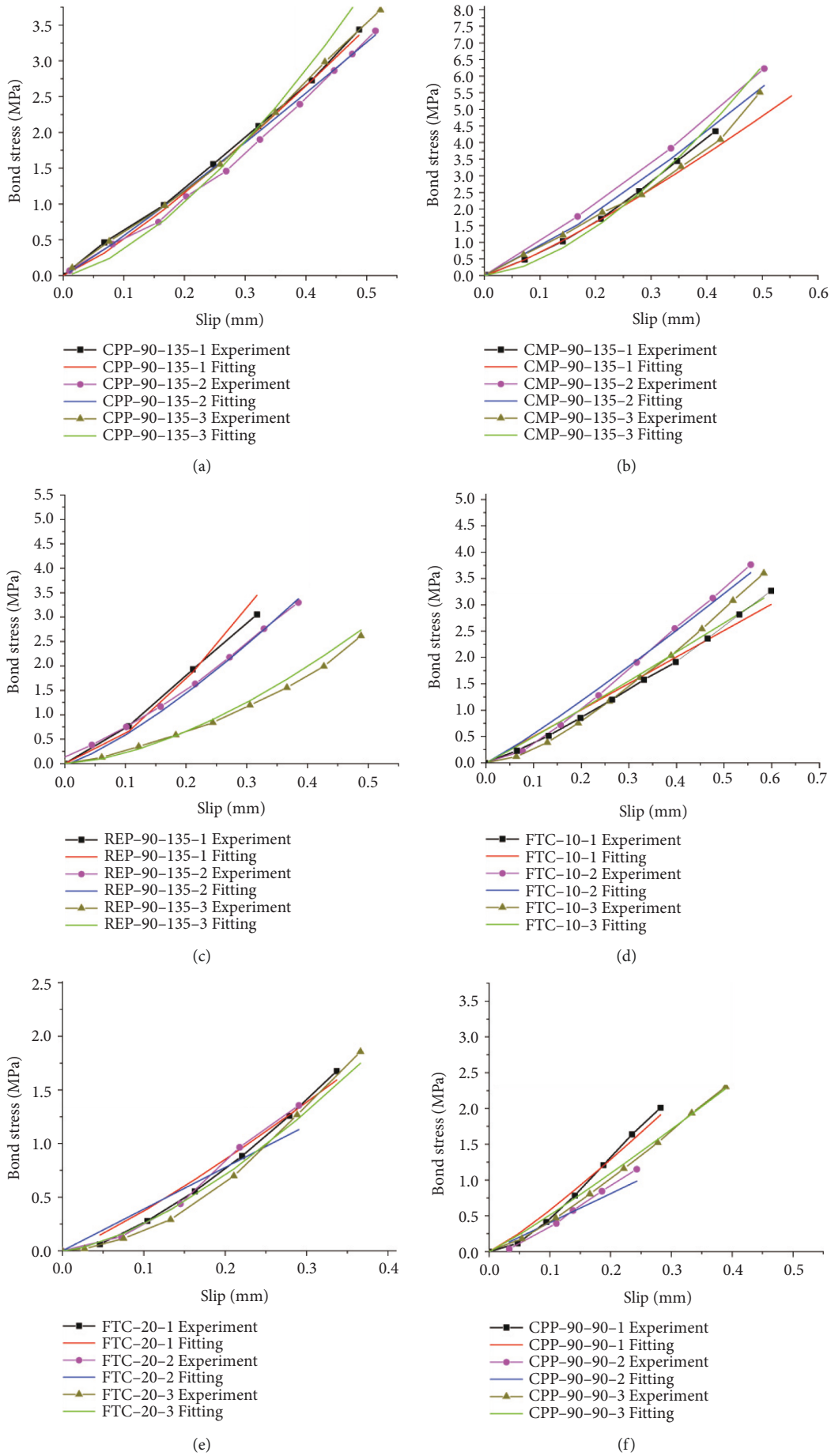

Figure 14: Continued.

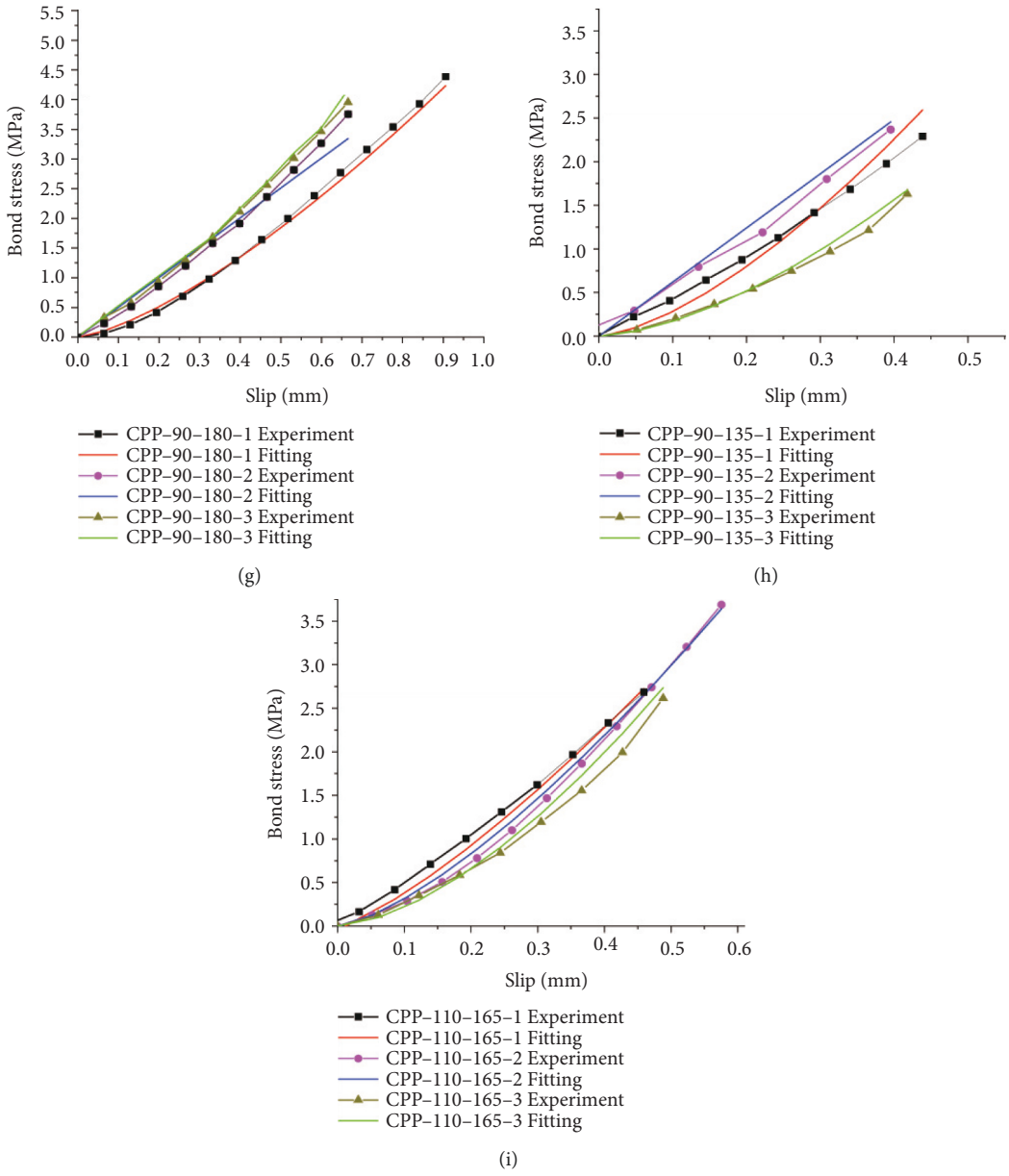

Figure 14: Comparison of theoretical results and fitting curves. (a) Cpp-90-135, (b) CMP-90-135, (c) REP-90-135, (d) CPP-FTC-10-135, (e) CPP-FTC-20-90-135, (f) CPP-90-90, (g) CPP-90-180, (h) CPP-80-112, (i) CPP-110-165.

$$\tau = \tau_s \left(\frac{S}{S_s}\right)^{\alpha}, \tag{3}$$

where S is the slip at the loaded end and τ is the average bond stress. The experimental results of the ultimate bond stress (τ_s) and ultimate slip (S_s) were used in this calculation. A comparison between the fitting data and experimental results is presented in Figure 14. A good agreement was observed in the ascending branch for all the specimens.

5. Conclusions

In this study, the relationship between force (bond stress) and displacement at the loading end was investigated using single-end compressive tests on grout-filled concrete components with multiple interface materials. The stronger the bond stress is, the greater the overall performance will be. Before the cracking of concrete structure, the stronger the bond stiffness is, the higher the bond strength to bond-slip ratio is, and the greater the ability of the diverse range of materials is to function together.

In support of the above, after experimental study, two types of curves were obtained: the axial load or stress of the first type of specimen reached peaks with a negative exponential distribution and then remained constant or increased linearly. The axial load or stress of the second type of specimens reached peaks with a negative exponential distribution, then increased linearly for a period, then increased to a new peak as a quadratic function, and finally remained constant. The specimens with rubber extractive pipes for

hole-forming included only the first type of curve. The specimens with corrugated metal and plastic pipes for hole-forming included both types of curves.

During specimen failure by loading, the corrugated metal pipe specimens were subjected to the highest pressure (and bond stress), followed by the corrugated plastic pipe specimens and the rubber extractive pipe specimens. The stiffness of the force curve (bond stress curve) was the highest for the corrugated metal pipe specimens, followed by the rubber extractive pipe and corrugated plastic pipe specimens. The critical displacement was the highest for the corrugated plastic pipe specimens, followed by the corrugated metal pipe and rubber extractive pipe specimens.

An increase in the number of freeze-thaw cycles reduced the load-bearing capacity of the specimen, bond stress curve, stiffness of the force curve, and stiffness of the bond stress curve. The reduction in these values for 20 freeze-thaw cycles relative to 10 freeze-thaw cycles was lower than that for 10 freeze-thaw cycles relative to 0 freeze-thaw cycles. For critical displacement, the reduction in value for 20 freeze-thaw cycles relative to 10 freeze-thaw cycles was higher than that for 10 freeze-thaw cycles relative to 0 freeze-thaw cycles.

The load-bearing capacity and bond stress increased significantly with an increase in the bond length. The stiffness of the force curve first increased and then remained almost constant, whereas the stiffness of the bond stress curve first increased and then decreased; the critical displacement increased gradually.

With an increase in bonding area, the load-bearing capacity and bond stress increased significantly. The stiffness of the force and displacement curves increased gradually, and the critical displacement increased gradually, but the increase was not significant.

The theoretical results are in good agreement with the experimental curves in light of peak loading force and peak bond stress, stiffness of loading force curve and bond stress curve, and bonding performance on critical displacement. From the perspective of peak loading force and peak bond stress, the bonding performance of the three hole-forming materials was ranked as follows: corrugated metal pipes > corrugated plastic pipes > rubber extractive pipes. From the perspective of the stiffness of the loading force curve and that of the bond stress curve, the bonding performance of the three types of hole-forming materials was as follows: corrugated metal pipes > rubber extractive pipes > corrugated plastic pipes. The bonding performance of the three materials was ranked based on critical displacement as follows: rubber extractive pipes > corrugated metal pipes > corrugated plastic pipes.

Data Availability

The data used to support the research are included within this manuscript.

Disclosure

Eryu Zhu and Teng Li should be regarded as co-first authors.

Conflicts of Interest

The authors declare that they have no known competing financial interests or personal relationships that could have influenced the work reported in this paper.

Authors' Contributions

Eryu Zhu and Teng Li contributed equally to this work.

Acknowledgments

The authors wish to express their gratitude to the Fundamental Research Funds for the Central Universities (Grant no. 2021JBM427).

References

[1] Y. Yu, *Experimental study on mechanical behavior of prestressed concrete beams with plastic sheath*, Ph.D. thesis, Southeast University, China, 2003.

[2] M. Zhou, Y. Huang, and B. Ge, "Some problems and suggestions in the application of corrugated plastic pipes for prestress concrete with bonds for hole-forming," *Jiangsu Transportation Research*, vol. 4, pp. 25–27, 2005.

[3] Z. Wang, "Application of corrugated plastic pipes in prestressed concrete bridges with bonds," *Plastics Industry*, vol. 44, no. 8, pp. 146–149, 2016.

[4] C. Gu, S. Chen, and S. Zhang, "Application of geo-radar in the grout plumpness detection of prestressed corrugated plastic pipes with bonds in box girder structures of prestressed concrete continuous rigid bridges with bonds," *Engineering Technology*, vol. 4, pp. 00267–00269, 2016.

[5] Y. Nie and B. Yu, "Hidden trouble and countermeasure of plastic bellows for prestressed concrete engineering," *Construction Technology*, vol. 5, pp. 29–32, 2009.

[6] X. Liu, Y. Liu, T. Wu, and H. Wei, "Bond-slip properties between lightweight aggregate concrete and rebar," *Construction and Building Materials*, vol. 255, Article ID 119355, 2020.

[7] X. Hu, G. Peng, D. Niu, X. Wu, and L. Zhang, "Bond behavior between deformed steel bars and cementitious grout," *Construction and Building Materials*, vol. 262, Article ID 120810, 2020.

[8] J. Khalaf and Z. Huang, "Analysis of the bond behaviour between prestressed strands and concrete in fire," *Construction and Building Materials*, vol. 128, pp. 12–23, 2016.

[9] S. Liu, H. Yuan, and J. Wu, "Full-range mechanical behavior study of FRP-to-concrete interface for pull-pull bonded joints," *Composites Part B: Engineering*, vol. 164, pp. 333–344, 2019.

[10] H. Yuan, J. G. Teng, R. Seracino, Z. S. Wu, and J. Yao, "Full-range behavior of FRP-to-concrete bonded joints," *Engineering Structures*, vol. 26, no. 5, pp. 553–565, 2004.

[11] Y. Chen, R. Feng, Y. Shao, and X. Zhang, "Bond-slip behaviour of concrete-filled stainless steel circular hollow section tubes," *Journal of Constructional Steel Research*, vol. 130, pp. 248–263, 2017.

[12] H. Dong, X. Chen, W. Cao, and Y. Zhao, "Bond-slip behavior of large high-strength concrete-filled circular steel tubes with different constructions," *Journal of Constructional Steel Research*, vol. 167, Article ID 105951, 2020.

[13] J. Song, W. Wang, S. Su, X. Ding, Q. Luo, and C. Quan, "Experimental study on the bond-slip performance between concrete and a corrugated steel plate with studs," *Engineering Structures*, vol. 224, Article ID 111195, 2020.

[14] F. Tariq and P. Bhargava, "Bond-slip models for super ductile TMT bars with normal strength concrete exposed to elevated temperatures," *Journal of Building Engineering*, vol. 32, Article ID 101585, 2020.

[15] L. Augusthus Nelson, M. Al-Allaf, and L. Weekes, "Analytical modelling of bond-slip failure between epoxy bonded FRP and concrete substrate," *Composite Structures*, vol. 251, Article ID 112596, 2020.

[16] Y. Cheng, *Experimental Study and Theoretical Analysis of the Interfacial Bond Performance of concrete-filled Square Steel Tube*, Ph.D. thesis, Xi'an University of Architecture and Technology, China, 2007.

[17] JGJ 52-2006, *Quality of Normal Concrete with Sand and Stone and Test Method Standard*, Chinese Standard, Beijing, China, 2006.

[18] GB 50204-2002, *Code for Construction Acceptance of Concrete Structure Engineering*, Chinese Standard, Beijing, China, 2002.

[19] TGE30-2005, *Test Methods of Cement and Concrete for Highway Engineering*, Chinese Standard, Beijing, China, (in Chinese), 2005.

[20] TB/T 3192-2008, *Technical Specification of Cable Grouts on Post-Prestressed Concrete Railway Girder*, Chinese Standard, Beijing, China, (in Chinese), 2008.

[21] GB/T 17671-1999, *Method of Testing Cements-Determination of Strength*, Chinese Standard, (in Chinese), 1999.

[22] GB/T. 8804.1-2003, *Thermoplastic Pipes-Determination of Tensile Properties-Part 1: General Test Method, 2003*, Chinese Standard, (in Chinese), 2003.

[23] O. Gooranorimi, W. Suaris, and A. Nanni, "A model for the bond-slip of a GFRP bar in concrete," *Engineering Structures*, vol. 146, pp. 34–42, 2017.

[24] K. He, Y. Chen, and S. Han, "Experimental investigation of square stainless steel tubular stub columns after elevated temperatures," *Journal of Constructional Steel Research*, vol. 159, pp. 397–414, 2019.

[25] Q. Hao, Y. Wang, and J. Hou, "Experimental study on bond behavior of GFRP ribbed rebars," *Engineering Mechanics*, vol. 25, no. 10, pp. 158–165, 2008.

[26] JB T 6169-2006, *Metal Bellows*, Chinese Standard, Chennai, India, 2006.

[27] Z.-H. Wang, L. Li, Y.-X. Zhang, and W.-T. Wang, "Bond-slip model considering freeze-thaw damage effect of concrete and its application," *Engineering Structures*, vol. 201, Article ID 109831, 2019.

[28] Y. Wang, F. He, J. Wang, and Q. Hu, "Comparison of effects of sodium bicarbonate and sodium carbonate on the hydration and properties of portland cement paste," *Materials*, vol. 12, no. 7, p. 1033, 2019.

[29] Y. Wang, F. He, J. Wang, C. Wang, and Z. Xiong, "Effects of calcium bicarbonate on the properties of ordinary Portland cement paste," *Construction and Building Materials*, vol. 225, pp. 591–600, 2019.

[30] Y. Pan and G. Xian, "Effects of freeze-thaw cycles on the behavior of the bond between CFRP plates and concrete substrates," *Journal of Composites for Construction*, vol. 22, no. 3, Article ID 04018011, 2018.

[31] A. Hosseini and D. Mostofinejad, "Effective bond length of frp-to-concrete adhesively-bonded joints: experimental evaluation of existing models," *International Journal of Adhesion and Adhesives*, vol. 48, pp. 150–158, 2014.

[32] J. Chen and J. Teng, "Anchorage strength models for FRP and steel plates bonded to concrete," *Journal of Structural Engineering*, vol. 127, no. 7, 2001.

[33] R. Seracino, M. R. Raizal Saifulnaz, and D. J. Oehlers, "Generic debonding resistance of eb and nsm plate-to-concrete joints," *Journal of Composites for Construction*, vol. 11, no. 1, pp. 62–70, 2007.

[34] Fédération Internationale du Béton (FIB), "Bulletin d'information no. 14," *Externally bonded FRP reinforcement for RC structures*, 2001.

[35] R. Eligehausen, E. Popov, and V. Bertero, "Local bond stress-slip relationships of deformed bars under generalized excitations: experimental results and analytical model," in *Proceedings of the Earthquake Engineering Research Center*, University of California, Berkeley, CA, USA, 1983.

[36] V. A. Rossetti, D. Galeota, and M. M. Giammatteo, "Local bond stress-slip relationships of glass fibre reinforced plastic bars embedded in concrete," *Materials and Structures*, vol. 28, no. 6, pp. 340–344, 1995.